Available online at www.sciencedirect.com
SCIENCE DIRECT
ELSEVIER
Journal of the European Ceramic Society 26 (2006) 2357–2364
ECERS
www.elsevier.com/locate/jeurceramsoc

Synthesis and characterization of $La_{0.85}Sr_{0.15}Ga_{0.85}Mg_{0.15}O_{3-\delta}$ electrolyte by steric entrapment synthesis method

Zhi-Cheng Li [a,*], Hong Zhang [b], Bill Bergman [a], Xiaodong Zou [b]

[a] *Department of Materials Science and Engineering, Royal Institute of Technology, SE 100 44, Stockholm, Sweden*
[b] *Structural Chemistry, Arrhenius Laboratory, Stockholm University, SE 106 91, Stockholm, Sweden*

Received 12 January 2005; received in revised form 20 April 2005; accepted 29 April 2005
Available online 24 June 2005

Abstract

Strontium and magnesium doped lanthanum gallate $La_{0.85}Sr_{0.15}Ga_{0.85}Mg_{0.15}O_{3-\delta}$ (LSGM) oxygen ionic conducting ceramics were prepared by a steric entrapment synthesis (SES) method, which is a polymeric precursor synthesis method by using polyvinyl alcohol in aqueous solution. The perovskite LSGM phase formed essentially at a calcination temperature of 900 °C. Pure and single perovskite LSGM phase with high relative density of 97.1% was obtained after sintering at 1450 °C, while the relative density of the LSGM sample sintered at the same temperature by solid state reaction (SSR) method was 80.6% in present experiment. Comparing with SSR synthesis method, the sintering temperature by SES can be reduced at least 100 °C. Impedance spectra revealed that the grain-boundary resistivity of LSGM synthesized by SES was smaller than that by SSR method, and the conductivities of the samples by SES were higher than those by SSR method at all measuring temperatures.

Keywords: (La,Sn) $(Ga,Mg)O_3$; Powders-chemical preparation; X-ray methods; Ionic conductivity

1. Introduction

Since the beginning of 20th century, more and more interest has been aimed at the fuel cells for the benefits of the efficient, silent and environmental-friendly properties for electric power generation. Among the various fuel cells, solid oxide fuel cells (SOFC) has attracted much attention because it offers various potential advantages, such as a wide variety of available fuels, a good durability, inexpensive technology and the potential advantage of higher efficiency. A typical SOFC has an electrolyte with 8 mol% yttria-stabilized zirconia (YSZ). YSZ-based SOFC is required to operate at high temperature of 800 °C–1000 °C. At high operating temperature, some harsh terms such as the sealing problem, thermal matches between materials and interface interaction between electrolyte and electrodes, etc., can be met, leading to higher manufacturing costs and application limitation for SOFC.[1] In order to reduce the operating temperature, some novel oxide ionic conductors including CeO_2-, Bi_2O_3- and $LaGaO_3$-based oxides have also been extensively investigated.[2–4] However, the problem of both CeO_2- and Bi_2O_3-based electrolytes is the reduction during operating, leading to the mixed electronic and ionic conductivity. Strontium- and/or magnesium-doped lanthanum gallate ceramics are the most promising electrolyte materials for intermediate temperature (IT) (500 °C–800 °C) SOFC applications. The properties such as oxide ionic conductivity, transference number of oxide ion and performance of $La_{1-x}Sr_xGa_{1-y}Mg_yO_{3-\delta}$ (LSGM, where $\delta = (x+y)/2$) ceramics at 650 °C are higher than those of the YSZ at 1000 °C.[5–7] The $LaGaO_3$-based ceramics have attracted much attention for the research and development of the electrolyte in the application of IT-SOFC.

According to the conventional solid state reaction (SSR) synthesis techniques, the formation of secondary phases (impurity phases) such as $LaSrGaO_4$ and $LaSrGa_3O_7$, long sintering time and Ga loss at high temperature are major hurdles for LSGM oxides preparation. One of the problems in the

* Corresponding author. Tel.: +46 8 790 8335; fax: +46 8 207 681.
E-mail address: zhchli@gmail.com (Z.-C. Li).

0955-2219/$ – see front matter © 2005 Elsevier Ltd. All rights reserved.
doi:10.1016/j.jeurceramsoc.2005.04.028

preparation of multiple-cation oxides is to get the homogeneous distribution of the cations in the mixed powder before calcinations and/or sintering. Besides the conventional synthesis method, several techniques have been reported for the preparation of LSGM materials: ultrasonic spray pyrolysis,[8] glycine-nitrate combustion synthesis,[9] sol–gel method,[10] Pechini method.[11] As reported by Kriven and coworkers,[12–15] a so-called steric entrapment synthesis method (SES) with inexpensive polymer, polyvinyl alcohol (PVA), is an efficient way for the preparation of mixed oxides. Highly reactive, highly sinterable, oxide powders have been synthesized by this method.[16] When this method was employed for the LSGM synthesis by Oncel and Gulgun,[17] $Ga_2(SO_4)_3$ was selected as one of the raw materials. After calcinations, no LSGM phase was observed by X-ray diffraction (XRD) from the precursor prepared with an exact stoichiometry composition. In the precursors with 10 wt.% and 20 wt.% excess gallium amounts, LSGM phase mixed with lanthanum sulfate and magnesium gallium oxide was found. Because lanthanum sulfate, which is stable at the calcination temperatures below 1200 °C, was formed, leading the existence of excess gallium, magnesium and strontium in the synthesized powder and the formation of stable impurity phase such as $MgGa_2O_4$. If all staring materials are metallic nitrates, it is possible that decomposition of the metallic nitrates takes place to metallic oxides and NO_2 at the temperature lower than 700 °C.

In this study, the steric entrapment synthesis method with nitrate salts as raw materials is employed to synthesize LSGM oxide. The results show that pure and single phase LSGM can be obtained, and the sintering temperature can be reduced about 100 °C to get high-density ceramics compared with solid state reaction synthesis. Besides, the conductivity of the LSGM oxides prepared by both SES and SSR are compared in this investigation.

2. Experimental procedure

The composition of LSGM was $La_{0.85}Sr_{0.15}Ga_{0.85}Mg_{0.15}O_{3-\delta}$. The steric entrapment synthesis method was performed as following. Calculated amounts of $La(NO_3)_3{\cdot}6H_2O$ (99.99%), $Sr(NO3)_2$ (99.97%), $Ga(NO_3)_3{\cdot}5H_2O$ (99.9%) and $Mg(NO_3)_2{\cdot}6H_2O$ (99.97%) (all of them were from Alfa Aesar, a Johnson Matthey Company, Germany) were dissolved separately in distilled water. Polyvinyl alcohol (PVA, 98–99%, Alfa Aesar, a Johnson Matthey Company, Germany) was dissolved in distilled water. Then the dissolved salt and PVA solutions were mixed in ratios such that there was one hydroxyl group of PVA for every cation in solution, resulting in the precursor solution. This mixed solution was heated at 250 °C while stirring until the water evaporated, as result, a crisp gel was obtained. The crisp gel was ground into a powder and put into ceramic crucibles. Calcination was performed in air in a tube furnace at temperatures from 700 °C to 1200 °C for 5 h, respectively. To compare with this synthesis method, conventional SSR method was also performed with raw materials of La_2O_3 (99.99%, Kebo AB, Sweden), $SrCO_3$ (>99.5%, Mallinkrodt chemical works, New York, USA), Ga_2O_3 (99.99%, Alfa Aesar, a Johnson Matthey Company, Germany) and $MgCO_3$ (>99.5%, Mallinkrodt chemical works, New York, USA). The raw materials were mixed by ball milling in alcohol according to the calculated amounts. After dried, the mixed powder was calcined at 1200 °C for 5 h in air.

The 1200 °C-calcined powders by both synthesis methods were granulated with polyvinyl alcohol and pressed into pellets with 15 mm diameter and 2.5 mm thickness. The pressure was 200 MPa. Sintering was performed for the SES-prepared samples at 1450 °C, 1500 °C and 1540 °C, respectively, for 5 h in a box furnace (model VMK 1800, Linn High Therm GmbH, Germany) in air. The samples prepared by SSR method were sintered, respectively, at 1450 °C, 1540 °C and 1580 °C for 5 h in air.

The phases of calcined powders and/or sintered samples by both methods were analyzed by X-ray powder diffraction (HUBER Imaging Plate Guinier Camera G670) with Cu Kα radiation, at room temperature. The sintered pellets were ground to a thickness of about 1 mm. Gold paste was painted on both parallel sides of the samples as the electrode. The ac conductivity of all the samples was characterized by an EI300 electrochemical impedance spectroscopy (Gamry Istruments, Inc.). The range of ac frequency is 0.01 Hz–300 KHz.

3. Results and discussion

3.1. Synthesis and microstructure

Fig. 1 shows the X-ray diffraction spectra of the $La_{0.85}Sr_{0.15}Ga_{0.85}Mg_{0.15}O_{3-\delta}$ powder prepared by SES and SSR methods, calcined at various temperatures. It can be seen that no perovskite LSGM phase can be detected in the 700 °C-calcined powder prepared by SES method. When the calcination temperatures are higher than 900 °C, strong peaks from the LSGM phase can be observed in these XRD spectra. Some peaks from the impurity phase instead of LSGM can also been seen from all the XRD spectra. The peak number from the impurity phases becomes less and the peak intensity becomes smaller when the calcinations temperature increases. The intensity ratio of the most intense peaks from the impurity phases over the total XRD intensity are 27.3%, 19.4%, 17.2% and 11.3% for the calcinations temperatures of 900 °C, 1000 °C, 1100 °C and 1200 °C, respectively. This implies that the amount of the impurity phases in the precursor powders decreased when the calcination temperature increased. Please note, when we calculated the intensity ratios, we just considered the intensities at the each peak tip, and did not take into account of the width of each peaks. Similar calculation was taken in the following intensity ratio calculation. Compared with the SES prepared powders, the SSR prepared powder calcined at 1200 °C (the

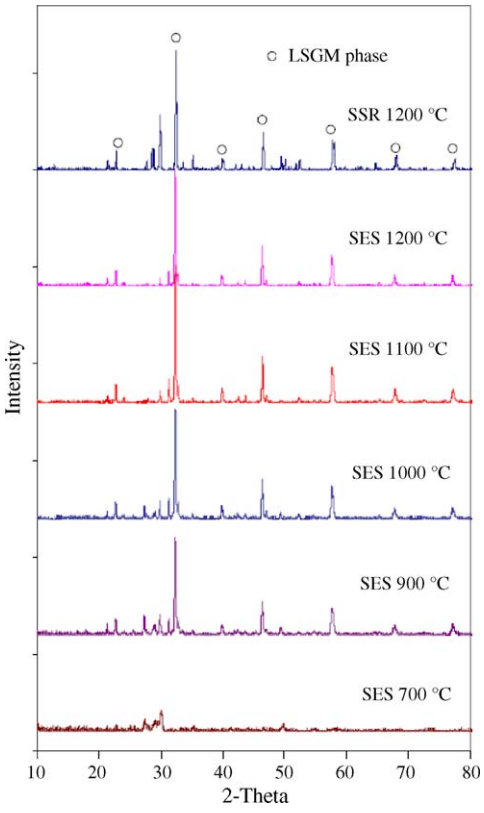

Fig. 1. X-ray powder diffraction analysis of calcined LSGM powders prepared by steric entrapment synthesis and solid state reaction synthesis.

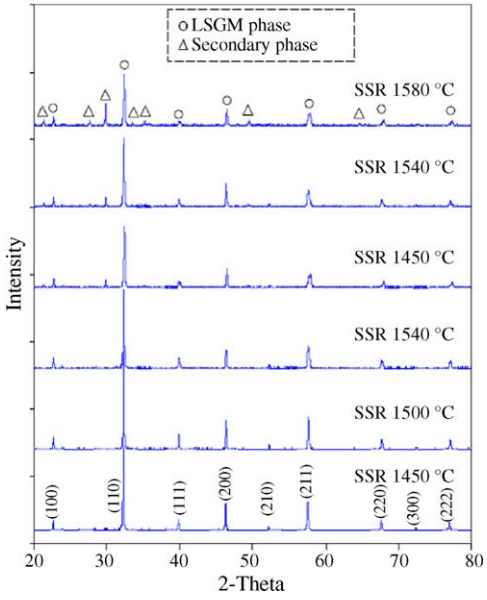

Fig. 2. X-ray powder diffraction analysis of sintered LSGM prepared by steric entrapment synthesis and solid state reaction synthesis.

intensity percentage of impurity phase is 38.7%) consists much more impurity phases, although LSGM phase is also obviously detectable from the XRD spectra.

XRD analysis of the sintered samples is shown in Fig. 2. All the SES prepared samples consist of pure LSGM perovskite phase after sintering. LSGM phase was also obviously detected in the SSR prepared sample after sintering at 1450 °C, although one small spectrum peak from the impurity phase can be observed. However, the intensity of the secondary phases increased when the sintering temperatures were 1540 °C and 1580 °C. The intensity ratios of the impurity phases are 4.3%, 6.1% and 18.9% for the sintering temperatures of 1450 °C, 1540 °C and 1580 °C, respectively.

The impurity phases depend strongly on the preparation method and technology, and different impurity phases may appear in various synthesis methods.[7,8,18] Present experiments also revealed the similar phenomena. The XRD spectra peaks from the impurity phases locate at different positions (2θ) in the samples by different synthesis methods, indicating that different impurity phase formed. In order to determine the possible impurity phases in the calcined powders and the sintered ceramics in present experiments, Table 1 lists the 2θ values from the impurity phases in the powders calcined at 900 °C (noted by SES900) and 1200 °C (noted by SES1200) by SES method, and that calcined at 1200 °C (by SSR1200) and sintered at 1580 °C (by SSR1580) by SSR method, respectively. At the same time, some XRD 2θ values of the possible impurity phases in LSGM-based ceramics are listed. The 2θ values of the impurity phases were referred from the PCPDFWIN database.[19]

Compared with SES900, the impurity phases of $LaSrGa_3O_7$ and $La_4Ga_2O_9$ should not exist in the SES calcined powders. Compared with SES1200, the possible impurity phase is $LaSrGaO_4$. These meant that the possible impurity phase in the 1200 °C-calcined powder by SES method was $LaSrGaO_4$. For the low melting temperature (~1400 °C), $LaSrGaO_4$ should be in a liquid state at the sintering temperature of 1450 °C. Diffusion or redistribution may occur for the liquefied $LaSrGaO_4$ during sintering, resulting that the amount decreases or the liquefied phase promote stronger bonding between grains. So the sintered samples show pure LSGM phase or the impurity phase became undetectable in XRD analysis.

On the other hand, for the synthesis by SSR method, the possible impurity phases should be $LaSrGa_3O_7$ and/or $La_4Ga_2O_9$. Both $LaSrGa_3O_7$ and $La_4Ga_2O_9$ have high melting temperatures (>1600 °C and >1900 °C, respectively). They are stable and can exist in the samples after sintering.

Although almost pure and single LSGM phase was obtained in the samples prepared by both SES and SSR methods sintered at the temperature of 1450 °C, the relative densities of the pellets by the two ways showed much difference. The relative densities are shown in Table 2. The relative density was determined by dividing the bulk density of the samples by the theoretical density. The theoretical density, which is 6.47 g/cm^3, was calculated by using the lattice parameters obtained from the XRD analysis: $a = 0.39075$ nm. It can be seen, from this table, that the pellet sintered at 1450 °C by SES has a higher density (97.1% relative density),

Table 1
2θ values of the possible impurity phases in LSGM ceramics, comparing to that of the impurity peaks of the powders calcined at 900 °C (SES900) and 1200 °C (SES1200) by SES method, and of that calcined at 1200 °C (SSR1200) and sintered at 1580 °C (SSR1580) by SSR method, respectively

Impurity	2θ (°) (by Cu Kα radiation)									
SES900	27.45–27.78	28.89–29.23	29.98–30.10	31.30–31.43			42.70	47.26	49.62–49.67	
SES1200			29.99–30.15	31.38–31.42			42.72	47.26		
SSR1200	27.80		29.96		33.73–33.80	35.36–35.42			49.62–49.77	50.19, 50.70
SSR1580	27.82		29.94		33.73–33.80	35.36–35.42			49.67–49.85	50.34
$LaSrGa_3O_7$	27.73		29.91			35.44			49.66	50.64
$La_4Ga_2O_9$	27.70, 27.94				33.76, 33.79					50.12, 50.62
La_2SrO_x	27.25, 27.94			31.59					49.79	
La_2MgO_x	27.25, 27.95			31.58					49.79	
$Sr_3Ga_2O_6$	27.68		29.91	31.42					49.70	
$Sr_3Ga_4O_9$		29.02	29.94		33.71					
$LaGa_{11}MgO_{19}$			29.55	31.47						
$LaSr_2Ga_{11}O_{20}$			29.99	31.38		35.39				50.09
$LaSrGaO_4$				31.45			42.71	47.28		

but the density of the pellet sintered at the same temperature by SSR method has much lower density (80.6% relative density). For the other temperature-sintered samples, the SES samples have similar relative densities.

According to the XRD analysis and relative densities as described above, SES synthesis should be an efficient synthesis method for the LSGM material preparation, comparing with the SSR method. Although dense and pure LSGM materials could be obtained by SSR method,[7] e.g. using regrinding, ball milling and longer sintering time, the processing is not as simple as that of SES method mentioned above. It is generally accepted that synthesis of ceramics by wet-chemical method is preferred to those employing reaction in the solid state, because it gives rise to more homogeneous powders with controlled composition. The steric entrapment synthesis method, a polymerized organic–inorganic route, that uses simple, long-chain polymers such as PVA as the carrier phase is a viable, simple, inexpensive technique for producing mixed-oxide powders,[20] in comparison with other wet-chemical methods such as the Pechini method. These simple polymer chains have no special chelating end groups, in contrast to the α-pyroxycarboxylic acid of the Pechini precursor. In aqueous PVA solutions, metal ions can be stabilized by the polymer via interaction with the hydroxyl groups. Even if some cations do not have a direct link to the hydroxyl groups, they are localized around the polymer by the bridging action of the water molecules between the metal ions that are linked to the hydroxyl groups and the free-floating metal ions. During precursor processing, the water of solution evaporates, the free space between the polymer molecules shrinks and the chain entanglement causes a close polymer. The cation mobility is greatly reduced and the water remained in the precursor still keeps all the cations in the entanglement polymer network. As a result, there is no precipitation to cause off-stoichiometry, and homogeneous powders can be obtained. By SSR synthesis method, it is impossible to get precursors with homogeneous chemical composition, the phase besides LSGM perovskite phase may form during calcination and sintering.

3.2. Impedance spectra

Electrical properties of all samples were characterized by ac impedance measurement. Generally, an impedance spectrum for the LSGM pellet is composed of three parts, a bulk (grain) semicircle, a grain-boundary semicircle and an electrode-process arc, which result from the bulk (grain), grain boundaries and electrolyte/electrode interfaces, respectively. Fig. 3 shows some impedance spectra, Nyquist plot, recorded at 200 °C of the samples prepared by both methods. In the 1450 °C-sintered sample by SES method, it consists of bulk semicircle, depressed grain-boundary semicircle and electrolyte/electrode interfacial part.

Some equivalent electrical circuits, as shown in Fig. 4a, were used to fit the impedance plots measured at 200 °C in the sample sintered at 1450 °C by SES method. Circuit A with bulk resistance (R_b) and bulk capacitor (C_b) is selected for fitting the bulk-part impedance. Circuit B consisting of bulk resistance (R_b), bulk capacitor (C_b) and constant phase element (CPE) is also used for fitting the bulk-part impedance. Circuit C has bulk resistance (R_b), bulk capacitor (C_b) and constant phase element (CPE) in grains for the bulk part,

Table 2
The relative densities and activation energies of the samples prepared by SES method and SSR method sintered at different temperatures

Synthesis method	SES			SSR		
Sintering temperature (°C)	1450	1500	1540	1450	1540	1580
Relative density (%)	97.1	97.0	96.8	80.6	95.8	96.0
E_a at 200 °C–500 °C (eV)	0.94	0.95	0.95	0.92	0.96	0.96
E_a at 500 °C–700 °C (eV)	0.68	0.67	0.68	0.61	0.68	0.78[a]

[a] The E_a was calculated at the temperatures between 600 °C and 700 °C.

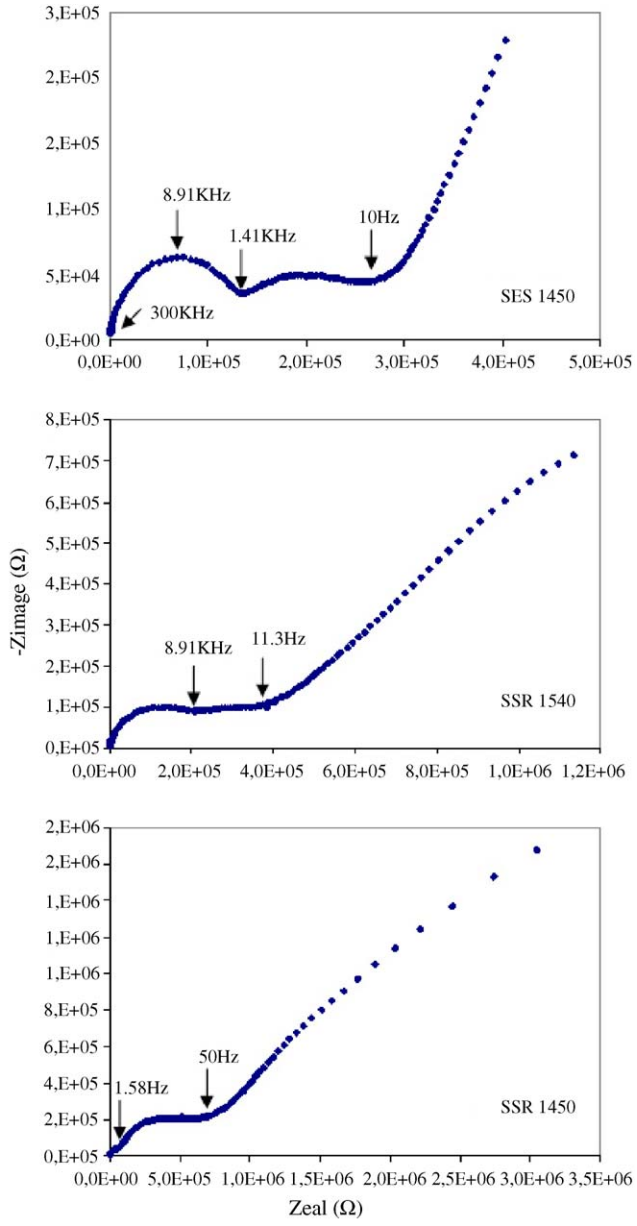

Fig. 3. Impedance spectra at 200 °C for the LSGM samples synthesized by SES and SSR methods.

and with grain-boundary resistance (R_{gb}), grain-boundary capacitor (C_{gb}) and constant phase element (CPE_{gb}) from grain boundaries for the grain-boundary part. Where a CPE's impedance is given mathematically by

$$\frac{1}{Z} = Q^{o}(j\omega)^{n}$$

where Q^{o} has the numerical value of the admittance ($1/Z^{*}$), and its unit is $S{\cdot}s^{n}$; n is CPE exponent ($0 < n \leq 1$). The fitted results for the real and imaginary parts in the impedance spectroscopic plots are shown in Fig. 4a. Plots A, B and C are gotten by the models of circuits A, B and C, respectively. At the same time, the relationships between frequency and impedance modulus, and between frequency and phase shift, were also used to check each fitting model, as shown in Fig. 4b.

Circuit A could not give a good fit. Even if we tried to adjust the values of resistance and capacity to get better fit, we still could not make the model to match well with the impedance (real and imaginary parts) and phases at the same time.

Circuit B gives a better fit than circuit A for all the impedance spectroscopic plots (the bulk part), impedance modulus and phase. Here, the effect from the grain boundaries was not included. The final fitted values are $R_b = 142\,k\Omega$ and $C_b = 1.2\,pF$, and $n = 0.925$ and $Q^{o} = 3.0 \times 10^{-10}\,S{\cdot}s^{n}$ for CPE.

Circuit C gives a good fit to both bulk part and grain-boundary part if the influence of electrode part was not considered. The final fitted values are $R_b = 140\,k\Omega$ and $C_b = 1.2\,pF$, and $n = 0.760$ and $Q^{o} = 5.0 \times 10^{-10}\,S{\cdot}s^{n}$ for bulk CPE; $R_b = 136\,k\Omega$ and $C_b = 95\,pF$, and $n = 0.7$ and $Q^{o} = 0.8 \times 10^{-9}\,S{\cdot}s^{n}$ for CPE_{gb}.

From the fitting results, the equivalent electrical circuits B and C are good models to fit the impedance, not only for the impedance real and imaginary parts, but also for the impedance modulus and phase. These meant that CPE exists in the samples. These fitted capacitance values (1.2 pF for the bulk and 95 pF for the grain-boundary) are in agreement with prior reports,[21,22] i.e. the capacitances for the bulk and grain-boundary components are of the order of 10^{-12} F and 10^{-11}–10^{-8} F, respectively.

The effect of CPE can be explained by various phenomena, depending on the nature of the system being investigated. However, the common thread among theses explanations is that some properties of the system are not homogenous or that there is some dispersion of the value of physical property of the system.[23,24]

On the other hand, the resistances from the grain boundaries are different in the samples prepared by the two methods as shown in Fig. 3. The sample sintered at 1450 °C by SSR method shows the largest resistance (the resistivity is about 3.81 MΩ cm), the SES sintered sample has the smallest grain-boundary resistance (the resistivity is about 0.95 MΩ cm). The sample sintered at 1540 °C prepared by SSR method also shows higher grain-boundary resistance. Large grain-boundary resistance should result from the relatively low density, the impurity phase, and/or defects existing at grain boundaries. In general, the impurity phases are always insulators or protonic conductors. For example, $LaSrGa_3O_7$ is one of the main impurity phases in SSR prepared samples, and is considered to be a protonic conductor under a hydrogen-containing atmosphere.[25] This indicates that the LSGM synthesis by steric entrapment method is favorable for the reduction of impurity phases and for improving the electrical properties.

Fig. 5 shows a series of impedance spectra of the 1450 °C SES-prepared sample measured at various temperatures. The impedance spectrum measured at 300 °C is composed of two depressed semicircles and an arc. For the frequency limitation

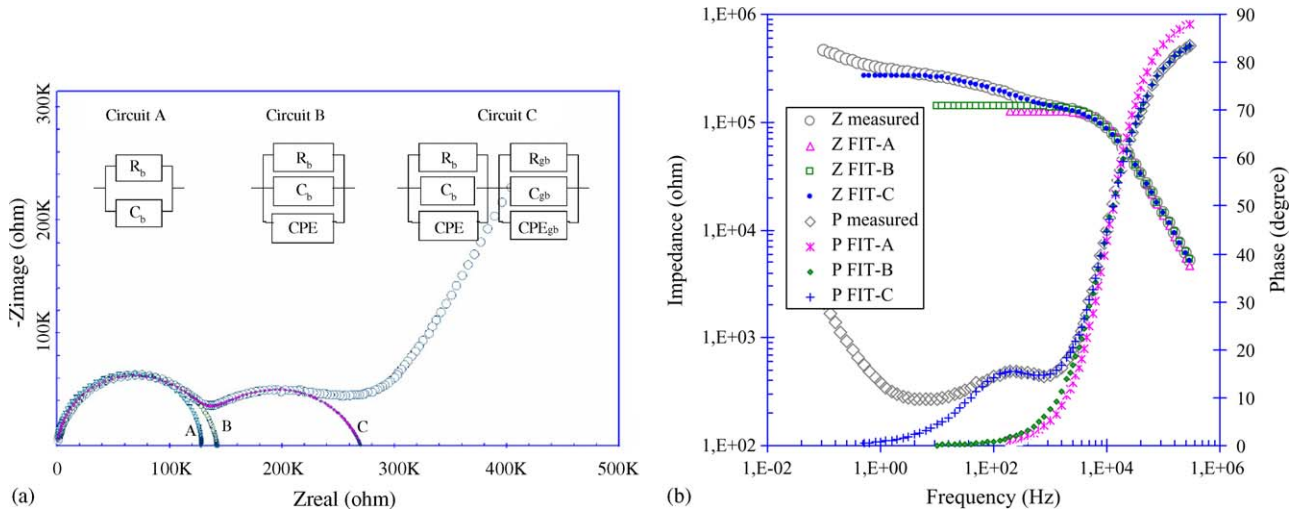

Fig. 4. Fit simulations of equivalent electrical circuits A, B and C for the impedance plots at 200 °C for the sample prepared by SES. (a) The fitted plots marked by A, B and C are for the models A, B and C, respectively. (b) Spectroscopic plots of impedance modulus (*Z* measured) and its related phase (*P* measured) as well as the fitted results by models A, B and C.

of the impedance spectroscopy, the first semicircle corresponding to the grain shows only one part instead of whole semicircle. The grain-boundary semicircle vanished at the temperature of 400 °C and consists of part of a depressed semicircle and an arc. The semicircle and arc are related to grain conduction and electrode/electrolyte interfaces conduction, respectively. With the increasing of temperature, the semicircle becomes small until totally disappears; only one arc which comes from the ion and electron transference between the electrode/electrolyte interfaces remains.

3.3. Conductivities

Fig. 6 shows Arrhenius plots of conductivity for the LSGM samples prepared by SES and SSR methods. At each measuring temperature, the conductivity of the samples synthesized by SES is higher than those of the samples prepared by SSR

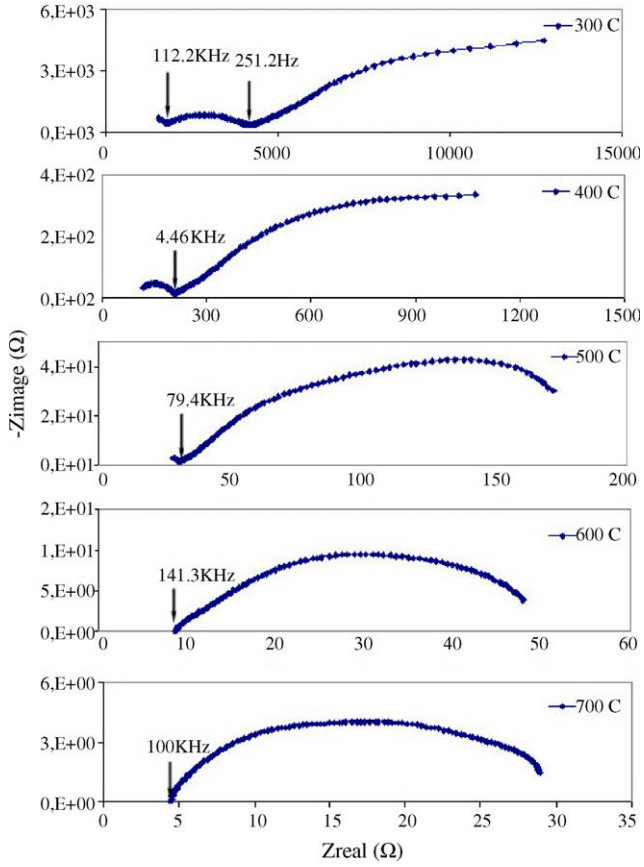

Fig. 5. Impedance spectra of a SES-prepared sample sintered at 1450 °C, measured at the temperatures 300 °C–700 °C.

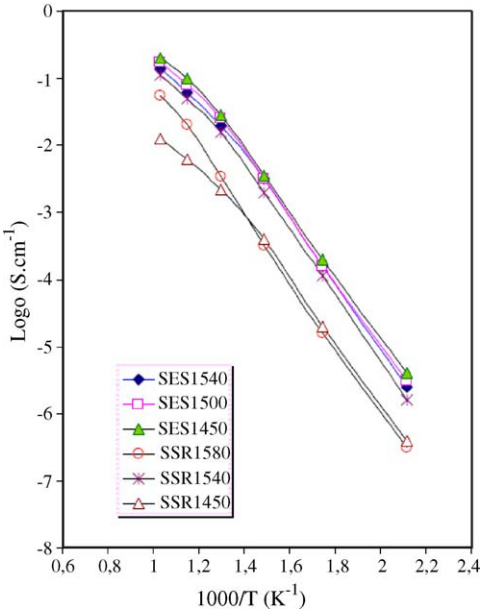

Fig. 6. Arrhenius plots of the LSGM samples prepared by SES and SSR methods.

method. This should result from the higher relative density and pure/single LSGM phase in the SES-synthesized sample, as shown in Fig. 2 and Table 1. The SES sample sintered at 1450 °C has the highest conductivity at all measured temperatures. Meanwhile, the conductivities of the other two SES samples, sintered at 1500 °C and 1540 °C, respectively, are little less than those of 1450 °C sintered sample. At the measured temperature range of 500 °C–700 °C, the sample sintered at 1450 °C prepared by SSR method has a much lower conductivity.

When made the conductivity plots by $\log(\sigma T)$ to $1/T$ (not shown here), we found that the plotted curves show straight lines and nearly parallel each other in all samples measured at the temperatures 200 °C–500 °C. This means they have similar activation energies, E_a, at that temperature range. All the calculated activation energies are shown in Table 2. They are similar to the value of 0.998 eV for LSGM ceramics with the same composition reported by Huang et al.[7] On the other hand, the conductivity plots for all samples do not show parallel lines at higher temperatures, indicating that the activation energies are different from each other. Meanwhile, the activation energy is smaller than that at lower temperatures for each sample. As reported by Huang et al.,[7] the dopant ions act not only as traps for isolated oxygen vacancies, but also as nucleating sites for the formation of ordered-vacancy clusters. At lower temperatures, the oxygen vacancies are progressively trapped out into the clusters; at higher temperatures, the vacancies can be dissolved into the matrix of the oxygen sites. The porosities can also catch the oxygen ions and affect the conductivity. In this case, the pores are trapped in the grains or grain boundaries, blocking oxygen ion migration, resulting in the lowest conductivity.

On the other hand, although the samples sintered at 1540 °C and 1580 °C by SSR method have the similar relative density, the sample sintered at higher temperature shows lower conductivity. The higher sintering temperature may lead to the occurrence of more secondary impurity phases (see Fig. 2), which block the oxygen ion migration because they are not ionic conductor. From the present investigation, the density of the sample and the existence of impurity phases should be the main factors influencing on the conductivity of LSGM.

4. Conclusion

A simple solution-polymerization method based on steric entrapment of cation within the polymer network was selected to prepare Sr- and Mg-doped lanthanum gallate $La_{0.85}Sr_{0.15}Ga_{0.85}Mg_{0.15}O_{3-\delta}$ (LSGM) ceramics. The analysis by X-ray powder diffraction revealed that mainly perovskite LSGM phase is formed when calcined at 900 °C, and pure perovskite LSGM phase with high relative density of 97.1% was obtained after sintering at 1450 °C. Comparing with solid state reaction synthesis method, the sintering temperature by steric entrapment synthesis method can be reduced at least 100 °C. The conductivities of the samples prepared by steric entrapment synthesis method are higher than that of the samples synthesized by solid state reaction method. The steric entrapment synthesis method is effective way for the synthesis of strontium and magnesium doped lanthanum gallate.

References

1. George, R. A. and Bessette, N. F., Reducing the manufacturing cost of tubular solid oxide fuel cell technology. *J Power Sources*, 1998, **71**, 131–137.
2. Kudo, T. and Obayashi, H., Mixed electrical conduction in fluorite-type $Ce_{1-x}Gd_xO_{2-x/2}$. *J Electrochem Soc*, 1976, **123**, 415–419.
3. Batle, P. D., Catlow, C. R. A., Heap, J. W. and Moroney, L. M., Structural and dynamic studies of delta-Bi_2O_3 oxide ion conductors: I. The structure of $(Bi_2O_3)_{1-x}(Y_2O_3)_x$ as a function of x and temperature. *J Solid State Chem*, 1986, **63**, 8–15.
4. Ishihara, T., Shibayama, T., Ishikawa, S., Hosoi, K., Nishiguchi, H. and Takita, Y., Novel fast oxide ion conductor and application for the electrolyte of solid oxide fuel cell. *J Eur Ceram Soc*, 2004, **24**, 1329–1335.
5. Ishihara, T., Matsuda, H. and Takita, Y., Doped $LaGaO_3$ perovskite type oxide as a new oxide ionic conductor. *J Am Ceram Soc*, 1994, **116**, 1801–1803.
6. Huang, P. and Petric, A., Superior oxygen ion conductivity of lanthanum gallate doped with strontium and magnesium. *J Electrochem Soc*, 1996, **143**, 1644–1648.
7. Huang, K., Ticky, R. S. and Goodenough, J. B., Superior perovskite oxide-ion conductor; strontium- and magnesium-doped $LaGaO_3$: I. Phase relationship and electrical properties. *J Am Ceram Soc*, 1998, **81**, 2565–2575.
8. Djurado, E. and Labeau, M., Secondary phases in doped lanthanum gallate perovskites. *J Eur Ceram Soc*, 1998, **18**, 1397–1404.
9. Cong, L., He, T., Ji, Y., Guan, P., Huang, Y. and Su, W., Synthesis and characterization of IT-electrolyte with perovskite structure $La_{0.8}Sr_{0.2}Ga_{0.85}Mg_{0.15}O_{3-\delta}$ by glycine-nitrate combustion method. *J Alloys Compd*, 2003, **348**, 325–331.
10. Zha, S., Xia, C., Fang, X., Wang, H., Peng, D. and Meng, G., Processing and electrical properties of doped-$LaGaO_3$ by gelcasting. *Ceram Int*, 2001, **27**, 649–654.
11. Polini, R., Pamio, A. and Traversa, E., Effect of synthesis route on sintering behavior, phase purity and conductivity of Sr- and Mg-doped $LaGaO_3$ perovskites. *J Eur Ceram Soc*, 2004, **24**, 1365–1370.
12. Gulgun, M. A. and Kriven, W. M., A simple solution-polymerization route for oxide powder synthesis, in powder synthesis and shape forming processes. *Ceram Trans*, 1995, **62**, 57–66.
13. Lee, S. J. and Kriven, W. M., Crystallization and densification of nano-size amorphous cordierite powder prepared by a PVA solution-polymerization route. *J Am Ceram Soc*, 1998, **81**, 2605–2612.
14. Nguyen, M. H., Lee, S. J. and Kriven, W. M., Synthesis of oxide powders by way of a polymeric steric entrapment precursor route. *J Mater Res*, 1999, **14**, 3417–3426.
15. Benson, E. A., Lee, S. J. and Kriven, W. M., Preoaration of portland cement components by PVA solution polymerization. *J Am Ceram Soc*, 1999, **82**, 2049–2055.
16. Kriven, W. M., Lee, S. J., Gulgun, M. A., Nguyen, M. H. and Kim, D. K., Synthesis of oxide powder via polymeric steric entrapment, in innovative processing/synthesis: ceramics, glasses, composites III. *Ceram Trans*, 2000, **108**, 99–110.
17. Oncel, C. and Gulgun, M. A., Synthesis of LaSrXMg-oxide with X = Ga, Fe, or Cr, *Mat Res Soc Symp Proc* 2003, 756, FF4.12.1-6.
18. Majewski, P., Rozumek, M. and Aldinger, F., Phasee diagram studies in the systems La_2O_3-SrO-MgO-Ga_2O_3 at 1350–1400 °C in air with

emphasis on Sr and Mg substituted $LaGaO_3$. *J Alloys Compd*, 2001, **329**, 253–258.
19. PCPDFWIN Database, *JCPDS-International Centre for Diffraction Data*, 1996.
20. Gulgun, M. A., Nguyen, M. H. and Kriven, W. M., Polymerized organic–inorganic synthesi of mixed oxides. *J Am Ceram Soc*, 1999, **82**, 556–560.
21. Abram, E. J., Sinclair, D. C. and West, A. R., Electrode-contact spreading resistance phenomena in doped-lanthanum gallate ceramics. *J Electroceram*, 2001, **7**, 179–188.
22. Abram, E. J., Sinclair, D. C. and West, A. R., A strategy for analysis and modeling of impedance spectroscopy data of electroceramics: doped lanthanum gallate. *J Electroceram*, 2003, **10**, 165–177.
23. Mulder, W. H., Sluytes, J. H., Pajkossy, T. and Nyikos, I., Tafel current at fracture electrode, connection with admittance spectra. *J Electroanal Chem*, 1990, **285**, 103–107.
24. Schiller, C. A. and Strunz, W., The evaluation of experimental dielectric data of barrier coating by means of different models. *Electrochim Acta*, 2001, **46**, 3619–3625.
25. Huang, K., Ticky, R. S. and Goodenough, J. B., Superior perovskite oxide-ion conductor; strontium- and magnesium-doped $LaGaO_3$: II. ac impedance spectroscopy. *J Am Ceram Soc*, 1998, **81**, 2576–2580.